Impact Bending of a Rotating, Rigid-Plastic Fan Blade

Tadashi Shioya*
University of Tokyo, Tokyo, Japan
and
William James Stronge†
University of Cambridge, Cambridge, England, UK

Damage caused by bird impact on a blade in a rotating fan has been idealized as transverse impact of a fluid jet on a semi-infinite, rigid-plastic beam with a centrifugal force acting parallel to the initial axis of the beam. In this preliminary dynamic analysis, the centrifugal force limits travel of the plastic hinges away from the impact point and decreases the deflection of the beam. A kink forms at the impact point; the amplitude of this kink is related to a moment of the impact force and is inversely proportional to the centrifugal force.

Introduction

JET engine fan blades can be damaged by impact with foreign objects injested into the engine. This damage is sometimes located near the impact point rather than at the root of a blade. Nonlinear structural analysis computer programs are being developed[1-6] to study the vibrational response and the three-dimensional indentation and cupping deformation observed in wide blade impact damage. However, for preliminary design, the general effect of engine design variables on dynamic response of blades to impact is still required.

The present analytical investigation is directed at the effect of centrifugal force on transverse plastic flexural of a blade caused by impact of a fluid mass. Previously, it was shown that in-plane flexural response to impact at the tip of a rigid-plastic blade is reduced by the centrifugal force.[7] For tip impacts, the largest bending curvature is close to the tip and inversely proportional to the centrifugal force. When impact is inside the tip, the deformation mode is more complex, progressing through a series of dynamic stages. This investigation is concerned with the effect of centrifugal force on blade bending in response to impact inside the tip.

Analytical Model

A blade in a rotating fan is subject to a radial body force gm per unit length, where m and g denote the mass density per unit length and the radial acceleration of the mass, respectively. The body force is caused by the centripetal acceleration $-g=r\omega^2$, where r is the radius and ω the angular speed of the fan. This analysis is concerned with damage near an impact location close to the blade tip in a rotating fan; since the change in radius across this region is small, the body force is assumed to be uniform. This steady force g acts parallel to the initial axis of the blade and toward the tip.

The dynamics of damage to a blade are represented as transient deformation around an impact point on a rigid, perfectly plastic beam which has a fully plastic yield moment M_0. The yield moment is assumed to be independent of the axial force, therefore, this beam represents only blades with thin cross sections. The blade is modeled as a uniform, semi-infinite beam; consequently, there is only one characteristic length in this analysis—the distance from the impact point to the tip, ξ. A transverse impact force F is applied to the beam at this location. This constant force represents the effect of a steady fluid jet acting on the blade a distance ξ from the tip.[7]

The effect of the impact force F and the uniform body force g will be represented by the nondimensional impact parameter α and centrifugal force parameter G.

$$\alpha=F\xi/M_0 \qquad G=gm\xi^2/M_0 \tag{1}$$

Nondimensional parameters for time t, length along the beam x, transverse deflection z, velocity $\dot{z}$, and acceleration $\ddot{z}$ may be defined in terms of the characteristic length ξ and moment M_0 as follows:

$$T=t\{M_0/(m\xi^3)\}^{1/2}, \qquad X=x/\xi, \qquad Z=z/\xi$$
$$\dot{Z}=\dot{z}(m\xi/M_0)^{1/2}, \qquad \ddot{Z}=\ddot{z}m\xi^2/M_0 \tag{2}$$

where $\dot{Z}=\mathrm{d}Z/\mathrm{d}T$ and $\dot{z}=\mathrm{d}z/\mathrm{d}t$. The resulting nondimensional moment is $M(X,T)$. As shown in Fig. 1, the nondimensional spatial coordinate X is measured from the tip of the beam, B.

Mode of Deformation

Impact away from the tip of a rigid-plastic beam results in three possible modes of deformation which depend only upon the magnitude of the impact moment about the tip. The three modes shown in Fig. 1 are required for the yield criterion to be satisfied throughout the beam.

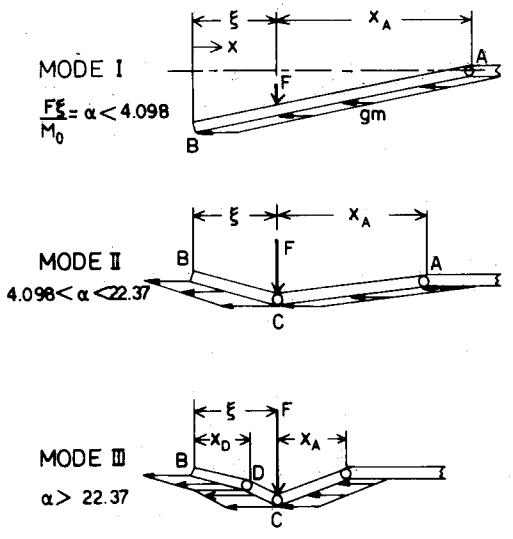

Fig. 1 Modes of deformation for rigid-plastic cantilever.

Received Oct. 30, 1984; revision received March 26, 1985.

*Associate Professor, Department of Aeronautics.
†Lecturer, University Engineering Department. Member AIAA.

Mode I: $0<\alpha<4.0981$

For low values of α, the deformation is essentially the same as for tip impact; a single hinge forms at A on the root side of the impact point. Since the hinge location is not specified, two equations of motion are required for this single hinge mode. When the inclination of the beam remains small, the transverse equation of motion is

$$\alpha=\int_{-1}^{X_A}\frac{d}{dT}\left[\dot{Z}_B\left(\frac{1+X_A-(1+\lambda)}{1+X_A}\right)\right]d\lambda \tag{3}$$

where X_A is the hinge distance from the impact point and $\dot{Z}_B$ is the transverse tip velocity. A second equation of motion can be established by taking moments about the tip of the beam, point B.

$$0=1+\alpha-\int_{-1}^{X_A}\lambda\frac{d}{dT}\left[\dot{Z}_B\left(\frac{1+X_A-(1+\lambda)}{1+X_A}\right)\right]d\lambda$$

$$-G\int_{-1}^{X_A}Z(\lambda)d\lambda \tag{4}$$

These equations of motion can be expressed more conveniently as

$$\ddot{Z}_B+\frac{\dot{X}_A\dot{Z}_B}{1+X_A}=\frac{2\alpha}{1+X_A} \tag{5}$$

$$\ddot{Z}_B+\frac{2\dot{X}_A\dot{Z}_B}{1+X_A}=\frac{}{(1+X_A)^2}\left\{1+\alpha+G\int_{-1}^{X_A}Z(\lambda)d\lambda\right\} \tag{6}$$

A plastic hinge within the beam can move so that at the hinge the bending moment $M=\pm1$ and $(d^2M/dX^2)[\text{sgn}\,(M)]\leq0$. The location of this hinge, X_A, can be determined from Eqs. (5) and (6). Since the centrifugal force acts parallel to the axis of an undamaged beam, the initial hinge location X_A can be determined from Eq. (6) by equating the integral on the right-hand side to zero.

$$X_A(0)=2+(3/\alpha) \tag{7}$$

Hence, the distance between the initial hinge location and the impact point is more than twice the distance between the tip and the impact point. Subsequently, this hinge moves away from the impact point with an initial acceleration

$$\ddot{X}_A(0)=G \tag{8}$$

As the plastic hinge moves along the beam, it leaves behind a curvature that depends on the angular velocity across the hinge and the traveling velocity of the hinge at the instant it traverses each particular location. Namely, the curvature $K(X_A)$ is expressed as

$$K(X_A)=\frac{\dot{Z}_B}{(1+X_A)\dot{X}_A} \tag{9}$$

With a constant force, the largest curvature occurs initially when

$$K_{max}=\frac{2\alpha^3}{9G(1+\alpha)^2} \tag{10}$$

In dimensional terms this largest curvature is $K_{max}=2F^3/\{9mg(F\xi+M_0)^2\}$, which is consistent with the case of impact at the tip, $\xi=0$.

The configuration of the beam as a function of time is calculated from Eqs. (5) and (6). By choosing GZ_B $[=gz_Bm\xi/M_0]$ and $\sqrt{G}T$ $[=(g/\xi)^{1/2}t]$ as the independent variables for tip deflection and time, the centrifugal force parameter G can be incorporated into the independent variables and, thus, one parameter is eliminated from the equations. In Figs. 2 and 3, the hinge distance from the tip $1+X_A$ and tip deflection GZ_B are shown as functions of time for two mode I values of the impact parameter α.

In mode I, the largest moment in the segment AB between the tip and the hinge is at C under the load where

$$M_C(T)=\int_0^1(1-\lambda)\frac{d}{dT}\left[\dot{Z}_B\left(\frac{1+X_A-\lambda}{1+X_A}\right)\right]d\lambda \tag{11}$$

This moment at C decreases with time from an initial value

$$M_C(0)=\frac{\alpha^2}{1+\alpha}\left\{\frac{1}{3}-\frac{\alpha}{27(1+\alpha)}\right\} \tag{12}$$

Mode I fails to satisfy the yield criterion throughout the beam if the moment at another section also equals the yield moment. When $M_C(0)=\pm1$, a second plastic hinge is formed at the point of impact.

The two-hinge mode of deformation is called mode II and occurs if

$$\alpha\geq(3+3\sqrt{3})/2\approx4.0981 \tag{13}$$

Mode II: $4.0981<\alpha<22.37$

When the impact parameter is larger than $3(1+\sqrt{3})/2$, a second hinge forms at the point of impact C. Thus, two rigid segments near the tip are separated by a plastic hinge at the impact point. The position of hinge A and the distribution of the impact force at C between the two segments are unknown; consequently, two equations of motion are required for each seqment.

For segment BC at the end of the beam, the equations for rate of change of transverse momentum and moment of momentum about point B are

$$F_T=(\ddot{Z}_B+\ddot{Z}_C)/2 \tag{14}$$

$$1=\int_0^1\lambda\frac{d}{dT}\{\dot{Z}_B+(\dot{Z}_C-\dot{Z}_B)\lambda\}d\lambda-G(Z_C-Z_B)/2 \tag{15}$$

where F_T is the shear force on the tip side of hinge C. A similar pair of equations of motion for segment CA (with the moment taken about C) are

$$F_R=\int_0^{X_A}\frac{d}{dT}\left[\frac{\dot{Z}_C(X_A-\lambda)}{X_A}\right]d\lambda \tag{16}$$

$$2=\int_0^{X_A}\lambda\frac{d}{dT}\left[\frac{\dot{Z}_C(X_A-\lambda)}{X_A}\right]d\lambda-G\left\{Z_C+\int_0^{X_A}Z(\lambda)d\lambda\right\} \tag{17}$$

where F_R is the shear force on the root side of hinge C. The sum of the shear forces is equal to the impact parameter.

$$F_T+F_R=\alpha \tag{18}$$

The equations of motion (14) to (18) can be reduced to

$$\ddot{Z}_B+(1+X_A)\ddot{Z}_C+\dot{X}_A\dot{Z}_C=2\alpha \tag{19}$$

$$2\ddot{Z}_B+\ddot{Z}_C=6\{1+G(Z_C-Z_B)/2\} \tag{20}$$

$$\ddot{Z}_C+\frac{2\dot{X}_A\dot{Z}_C}{X_A}=\frac{6}{X_A^2}\left\{2+G\int_0^{X_A}Z(\lambda)d\lambda\right\} \tag{21}$$

Initial conditions for the two segments are

$$Z_B(0)=\dot{Z}_B(0)=0,\qquad Z_C(0)=\dot{Z}_C(0)=0 \tag{22}$$

The hinge A is initially located at

$$X_A(0) = \{6 + 2\sqrt{3\alpha + 9/2}\}/(2\alpha - 3) \tag{23}$$

with initial traveling velocity $\dot{X}_A(0) = 0$. The initial accelerations of the tip and impact point are

$$\ddot{Z}_B(0) = 2(-\alpha - 3 + 2\sqrt{3\alpha + 9/2}) \tag{24}$$

$$\ddot{Z}_C(0) = 2(2\alpha + 9 - 4\sqrt{3\alpha + 9/2}) \tag{25}$$

As the hinge at A travels away from the tip, it leaves behind a curvature that decreases with distance. In contrast, the stationary hinge under the impact point has an infinitely large curvature. The change in angle of inclination across the impact point increases with time

$$\theta_C = \int_0^T \dot{\theta}_C(\tau)\,d\tau = \int_0^T \{(\dot{Z}_C - \dot{Z}_B) + \dot{Z}_C/X_A\}\,d\tau \tag{26}$$

Equations (19-21), with their initial conditions, have been calculated to obtain the deformation with time. These equations will determine the deflection parameters GZ_B and GZ_C as a function of the time parameter $\sqrt{G}T$, so the effect of the centripetal acceleration is incorporated into the parameters. The movement of the two hinges formed in the case of $\alpha = 10$ is shown in Fig. 2 alongside the movement of two hinges from smaller values of the impact parameter α. Deflections of the tip and impact point hinge are shown for the same set of mode I and mode II impacts in Fig. 3. Figure 4 shows the development of the kink at the impact point in mode II. After some time, the relative rotation at the hinge ceases when the moment at C is no longer as large as the yield moment; then the deformation reverts to mode I.

In mode II, the initial bending moment distribution in the segment BC is

$$M(\lambda) = \int_0^\lambda (\lambda - \eta)\frac{d}{dT}\{\dot{Z}_B + (\dot{Z}_C - \dot{Z}_B)\eta\}\,d\eta$$

$$= \lambda^3(\alpha + 4 - 2\sqrt{3\alpha + 9/2}) - \lambda^2(\alpha + 3 - 2\sqrt{3\alpha + 9/2}) \tag{27}$$

where λ is the distance from the tip. For $\alpha > 3 + \sqrt{3}$, this moment can be negative with a minimum at $\lambda_D = 2(\alpha + 3 - 2\sqrt{3\alpha + 9/2})/\{3(\alpha + 4 - 2\sqrt{3\alpha + 9/2})\}$. When $M(\lambda_D) = -1$ another plastic hinge forms within the end segment of the beam; this occurs at

$$\alpha = 22.37 \tag{28}$$

Mode III: $\alpha > 22.37$

When the impact parameter is very large, a third plastic hinge is formed located between the tip and impact point. The three plastic hinges separate three rigid segments of the beam, as shown in Fig. 1. Again, each segment requires two equations of motion since either the hinge location or the distribution of the impact force is not specified at the hinges.

For segment BD at the end of the beam, the equations of rate of change of transverse momentum and moment of momentum about B are

$$0 = \int_0^{X_D} \frac{d}{dT}\left\{\dot{Z}_B + (\dot{Z}_D - \dot{Z}_B)\frac{\lambda}{X_D}\right\}d\lambda \tag{29}$$

$$1 = \int_0^{X_D} \lambda\frac{d}{dT}\left\{\dot{Z}_B + (\dot{Z}_D - \dot{Z}_B)\frac{\lambda}{X_D}\right\}d\lambda$$

$$- G\left[\int_0^{X_D} \{Z(\lambda) - Z_B\}\,d\lambda + X_D\{X_D\theta_D - (Z_D - Z_B)\}\right] \tag{30}$$

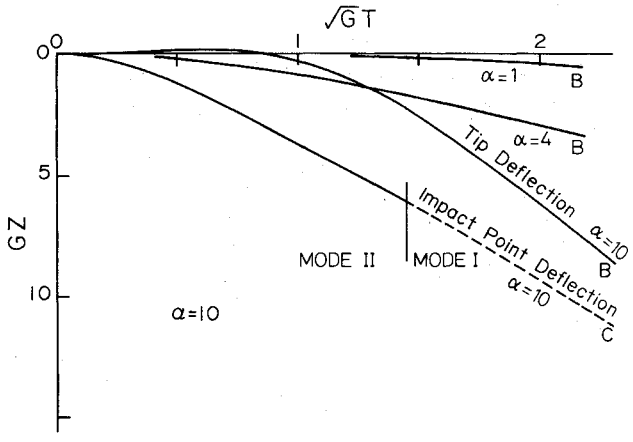

Fig. 3 Deflection of tip GZ_B [$= gz_B m\xi/M_0$] vs time parameter $\sqrt{G}T$ [$(g/\xi)^{1/2}t$] in modes I and II.

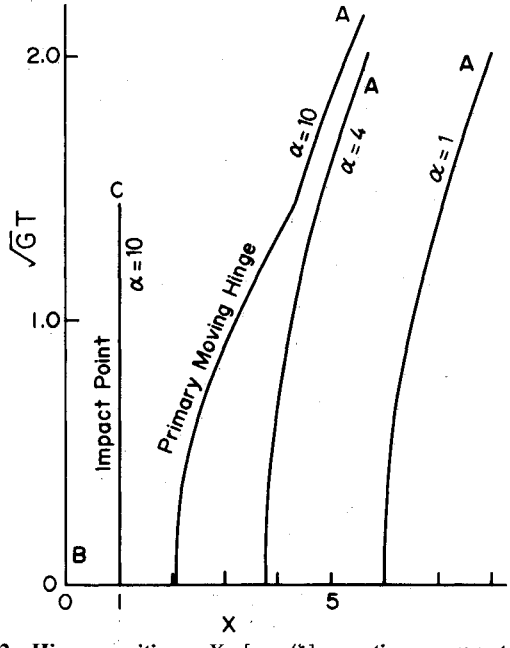

Fig. 2 Hinge positions X [$= x/\xi$] vs time parameter $\sqrt{G}T$ [$= (g/\xi)^{1/2}t$] in modes I and II.

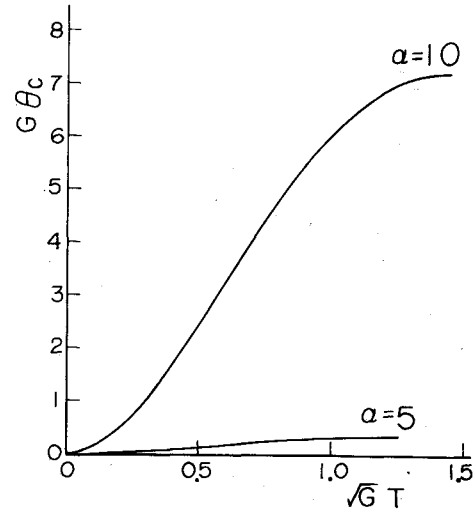

Fig. 4 Development of kink $G\theta_C = [gm\xi^2/M_0]\theta_C$ at impact point in mode II.

where X_D is the location of the third hinge measured from the tip and θ_D the inclination of the beam at D with respect to the initial axis. The other segment outside the impact point has a similar pair of equations when moments are taken about the impact point C.

$$F_T = \int_0^{1-X_D} \frac{d}{dT}\left\{\dot{Z}_D + (\dot{Z}_C - \dot{Z}_D)\frac{\lambda}{1-X_D}\right\}d\lambda \tag{31}$$

$$2 = \int_0^{1-X_D} (1-X_D-\lambda)\frac{d}{dT}\left\{\dot{Z}_D + (\dot{Z}_C - \dot{Z}_D)\frac{\lambda}{1-X_D}\right\}d\lambda + G\left[\int_0^{1-X_D}\{Z_C - Z(\lambda)\}d\lambda - X_D\{(1-X_D)\theta_D - (Z_C - Z_D)\}\right] \tag{32}$$

The segment inside the impact point has basically the same equations as in mode II, i.e.,

$$F_R = \int_0^{X_A} \frac{d}{dT}\left[\frac{\dot{Z}_C(X_A-\lambda)}{X_A}\right]d\lambda \tag{33}$$

$$2 = \int_0^{X_A} \lambda\frac{d}{dT}\left[\frac{\dot{Z}_C(X_A-\lambda)}{X_A}\right]d\lambda - G\left\{Z_C + \int_0^{X_A} Z(\lambda)d\lambda\right\} \tag{34}$$

In these equations, the sum of the shear forces is again equal to the impact parameter,

$$F_T + F_R = \alpha \tag{35}$$

These seven equations [Eqs. (29-35)] are solved numerically for the unknown hinge positions X_A and X_D, deflection parameters GZ_B, GZ_C, and GZ_D and shear forces F_T and F_R with the time parameter $\sqrt{G}T$. In mode III, both the hinges A and D move away from the impact point C. After some time, the deflection of the beam and the centrifugal force reduce the plastic rotation rate at hinge D. When the bending moment at D is no longer as large as the yield moment, the deformation reverts to mode II. After another period of time, the moment at C also becomes less than the yield moment and the deformation is finally mode I. In Figs. 5 and 6, the calculated hinge positions and the deflection parameters as functions of the time parameter are shown in the case of $\alpha = 100$. Figure 7 shows the increasing amplitude of the kink at the impact point.

Discussion

Transverse impact on a rigid-plastic cantilever causes deformation at discrete plastic hinges; the mode of deformation depends only on the magnitude of the impact moment about the tip (impact parameter α). The initial hinge positions are shown as a function of the impact parameter in Fig. 8. As α increases, the hinges form closer to the impact point; i.e., the highly deformed region becomes more localized. On the other hand, if α is small the deformed region is rather wide in this rigid-plastic model; elastic-plastic deformations are likely to be significantly different from this model in the case of small α.

If there is no centrifugal force, the hinge positions are stationary during constant loading and only move after the force is removed. In the presence of centrifugal force, the hinges

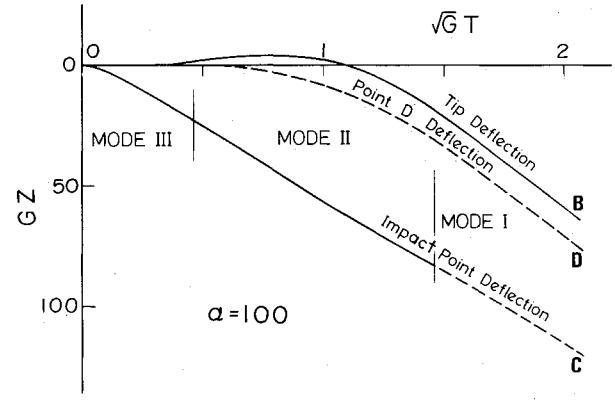

Fig. 6 Deflection of tip and hinges GZ [$=gzm\xi/M_0$] vs time parameter $\sqrt{G}T$ [$=(g/\xi)^{1/2}t$] in mode III.

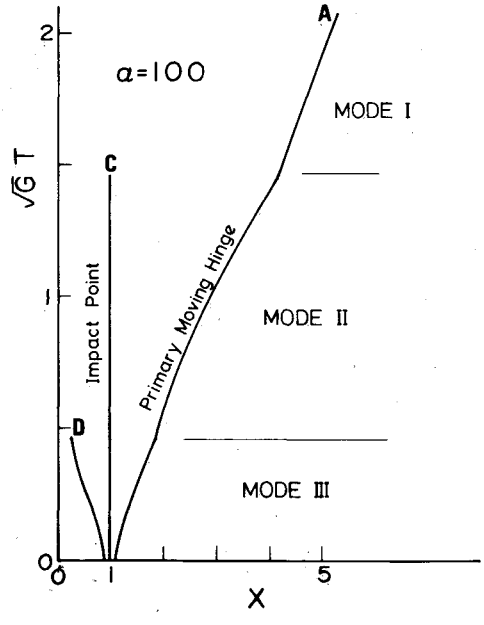

Fig. 5 Hinge positions X [$=x/\xi$] vs time parameter $\sqrt{G}T$ [$(g/\xi)^{1/2}t$] in mode III for α[$=F\xi/M_0$] = 100.

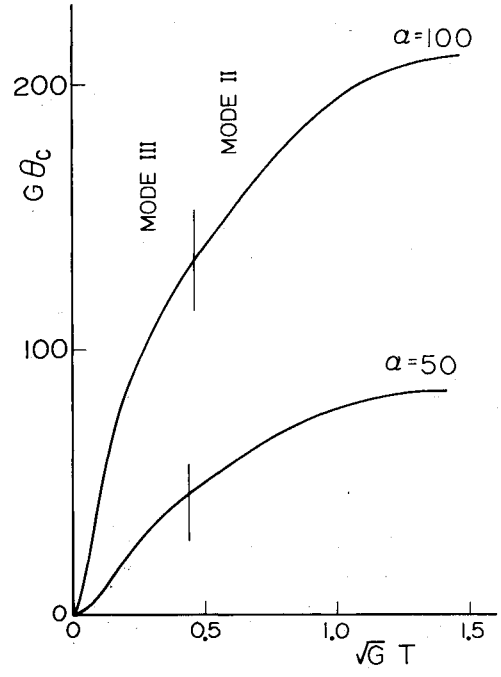

Fig. 7 Development of kink $G\theta_C = [gm\xi^2/M_0]\theta_C$ at impact point in mode III.

travel away from the impact point and the deformation mode changes with time even though the load is constant. The effect of the centrifugal force is to reduce the deflection and accelerate the transitions in mode of deformation.

When $\alpha > 3(1+\sqrt{3})/2$ a kink will be formed at the impact point. The discontinuity in inclination at this kink θ_C develops with time until it reaches an upper bound θ_{max} when the mode changes to mode I. The numerical analysis shows that this mode change occurs at about $\sqrt{G}T = 1.5$ regardless of α throughout modes II and III. The maximum kink angle θ_{max} is reciprocal to G and increases with α as shown in Fig. 9. This relation represents the influence of both impact and centrifugal forces on this damage criterion. Since the analysis postulates infinite duration of impact, θ_{max} is an upper bound on the kink angle.

The energy imposed by foreign object impact is proportional to the deflection at the impact point while the load is constant. The energy is partitioned to plastically dissipated energy E_P at the hinges and kinetic energy E_K of the moving segments. Figure 10 shows the variation of these energy parameters with time $\sqrt{G}T$ in each mode. Both the plastic and kinetic energies increase with time but the kinetic energy soon becomes dominant, especially in mode III. After the initial multiple hinge period of deformation, the residual kinetic energy exceeds the work in plastic deformation; however, the spatial distribution of that kinetic energy is unlikely to cause

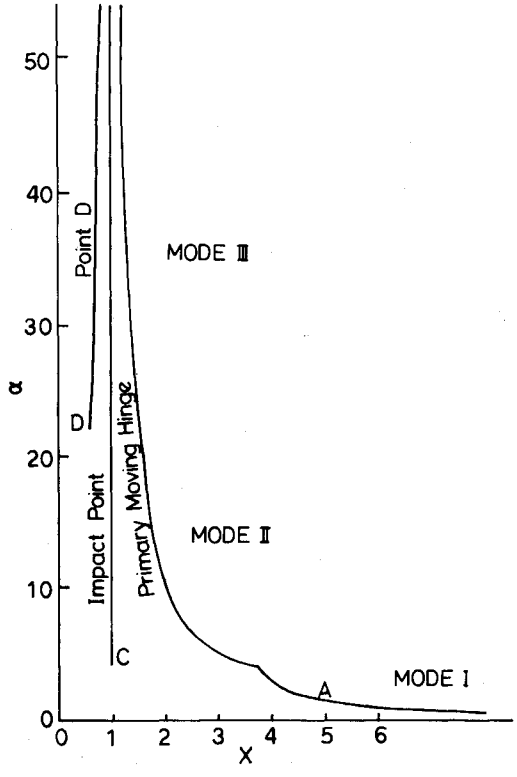

Fig. 8 Initial hinge location X $[=x/\xi]$ vs impact parameter $\alpha[F\xi/M_0]$.

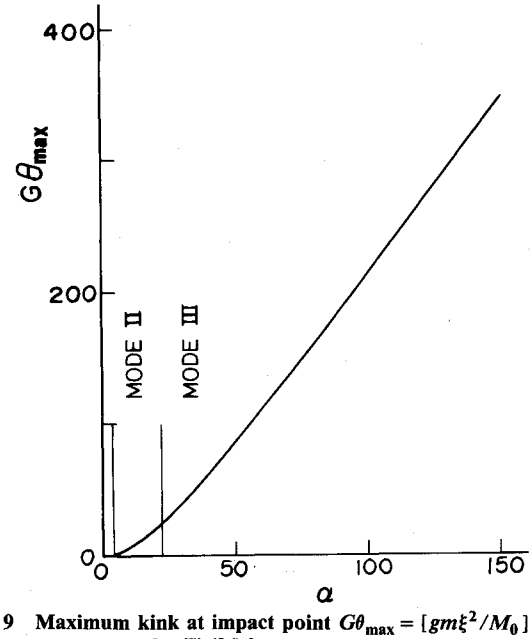

Fig. 9 Maximum kink at impact point $G\theta_{max} = [gm\xi^2/M_0]\theta_{max}$ vs impact parameter α $[=F\xi/M_0]$.

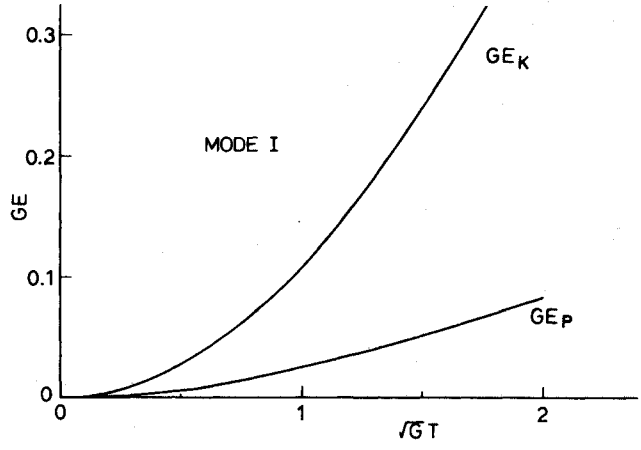

a) Mode I; $\alpha = 1$.

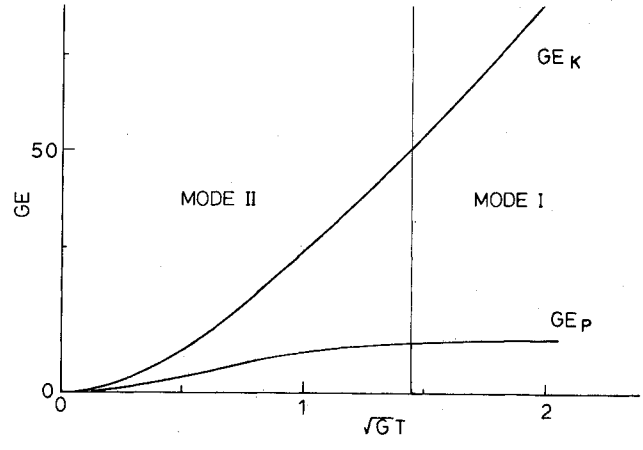

b) Mode II; $\alpha = 10$.

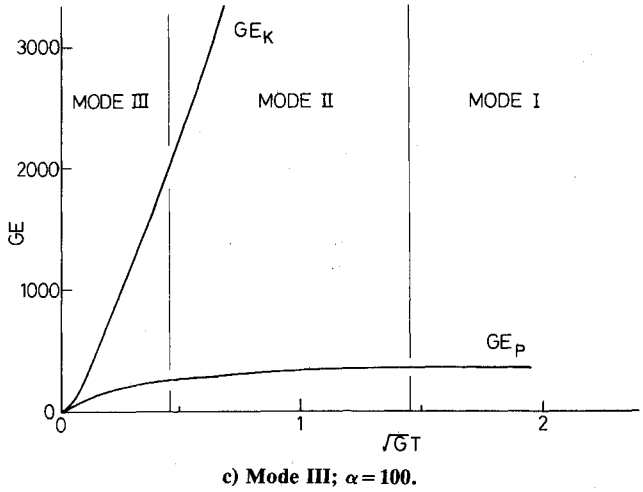

c) Mode III; $\alpha = 100$.

Fig. 10 Kinetic and plastic energy parameters GE_P, GE_K [=(energy)$\times gm\xi^2/M_0^2$] vs time parameter $\sqrt{G}T$ $[=(g/\xi)^{1/2}t]$

further plastic deformation near the point of impact. This suggests that the assumption of a rate independent yield stress in the analysis can be a satisfactory approximation when the impact parameter α is large.

In the present analysis, only the constant loading process is shown and unloading has been excluded. There is basically no difficulty in analyzing the process during unloading. The deflection of the beam continues to increase during this phase but the discontinuity at the impact point does not increase after unloading.

The physical problem of impact on rotating fan blades involves three-dimensional factors that result in nonuniform bending and twisting of the impact section. In blades that contain abrupt changes in section, deformations are focused at discontinuities where kinks can form away from the impact point.[8] None of these engine design details have been incorporated into the present analysis which is aimed at the effect of centrifugal force on dynamic plastic bending. Considerations of detail must finally be tackled in safety analyses by numerical methods.

The present analysis is based on one-dimensional uniform beam theory. If the beam has flaws or weak points, the mode of deformation can alter. If the impact is off the neutral axis of the beam, twisting occurs in addition to bending. The actual impact problem involves many three-dimensional factors both in the blade geometry and the position and orientation of the impact object, so that large-scale FEM codes become necessary to obtain quantitative values for engine design. The present analysis is not aimed toward direct application to design, but is directed toward understanding damageability in terms of basic design parameters.

Conclusions

Fluid impact on a rigid-plastic fan blade can cause three modes of deformation depending on the impact moment about the tip. Centrifugal force can be incorporated within the time and deflection parameters to concisely present the effect of fan rotation on impact damage near the tip. When the impact moment $\alpha > 4.1$, the largest curvature occurs at a kink located at the impact point. The discontinuity in inclination at this kink is an increasing function of only the impact parameter, $\alpha = F\xi/M_0$.

References

[1]Alexander, A., "Interactive Multi-Mode Blade Analysis," ASME Paper 81-GT-79, March 1981.

[2]Hirschbein, M.S., "Bird Impact Analysis Package for Turbine Fan Blades," NASA TM-82831, 1982.

[3]Bauer, D.P., "Response Sensitivity of Typical Aircraft Jet Engine Fan Blade-Like Structures to Bird Impacts," AFWAL-TR-82-2045, May 1982.

[4]Hirschbein, M.S. and Brown, K.W., "STAEBL—Structural Tailoring of Engine Blades (Phase II)," *Multidisciplinary Analysis and Optimization Symposium,* NASA Langley Research Center, April 1984.

[5]Aiello, R.A., Hirchbein, M.S., and Chamis, C.C., "Structural Dynamics of Shroudless, Hollow Fan Blades with Composite In-Lays," NASA TM-82816, 1982.

[6]Chamis, C.C. and Sinclair, J.H., "Analysis of High Velocity Impact on Hybrid Composite Fan Blades," NASA TM-79133, 1979.

[7]Stronge, W.J. and Shioya, T., "Impact and Bending of a Rigid-Plastic Fan Blade," *Journal of Applied Mechanics, Transactions of ASME* Vol. 51, Sept. 1984, pp. 501-504.

[8]Petroski, H.J., "The Permanent Deformation of a Cracked Cantilever Struck Transversely at Its Tip," *Journal of Applied Mechanics, Transactions of ASME*, Vol. 51, June 1984, pp. 329-334.